Biophysical Chemistry 192 (2014) 33–40

Contents lists available at ScienceDirect

Biophysical Chemistry

journal homepage: http://www.elsevier.com/locate/biophyschem

Ion-dynamics in hepatitis C virus p7 helical transmembrane domains — a molecular dynamics simulation study

Yi-Ting Wang [a,b], Roman Schilling [c], Rainer H.A. Fink [c], Wolfgang B. Fischer [a,b,*]

[a] Institute of Biophotonics, School of Biomedical Science and Engineering, National Yang-Ming University, Taipei, 112, Taiwan
[b] Biophotonics and Molecular Imaging Research Center (BMIRC), National Yang-Ming University, Taipei, 112, Taiwan
[c] Medical Biophysics Group, Institute of Physiology and Pathophysiology, University of Heidelberg, 69120 Heidelberg, Germany

HIGHLIGHTS

- Generation of hexameric assemblies of ion channel forming p7 of HCV
- Protonation of His-17 allows Cl-ions to enter the pore.
- In unprotonated bundle also Ca-ions are found within the pore.
- Applied voltage identifies large Cl-ion currents from the site of the loop.
- Slight rectification of the current is observed.

GRAPHICAL ABSTRACT

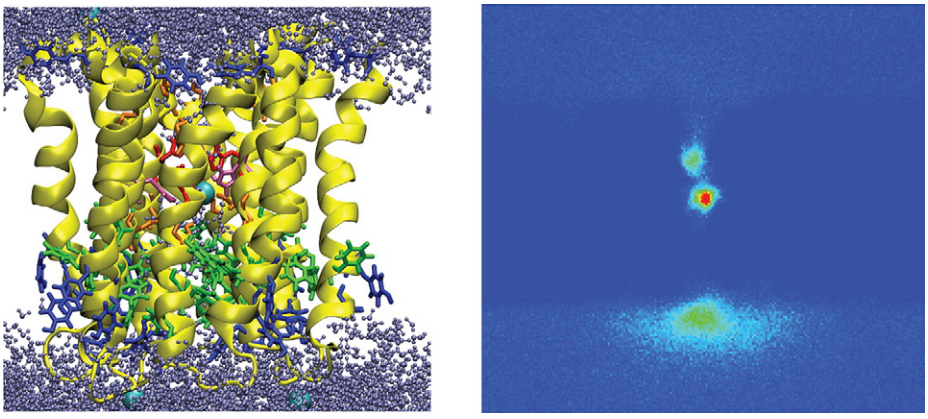

ARTICLE INFO

Article history:
Received 12 April 2014
Received in revised form 4 June 2014
Accepted 6 June 2014
Available online 16 June 2014

Keywords:
Membrane protein
Ion channels
Computational modeling
Protein structure
Conductance

ABSTRACT

Viral proteins assemble into homopolymers in the infected cells and have a role as diffusion-amplifier for ions across subcellular membranes. The homopolymer of hepatitis C virus, protein p7 of strain 1a, which is known to form channels, is used to investigate the dynamics of physiological relevant ions, Na^+, K^+, Cl^- and Ca^{2+} in the vicinity of the protein bundle. The protein bundle is generated by a combination of docking approach and molecular dynamics (MD) simulations. Ion dynamics are recorded during multiple 200 ns MD simulations of 1 M solutions. His-17 is found to point into the lumen of the pore. Protonation of this residue allows Cl-ions to enter the pore while in its unprotonated state Ca-ions are found within the pore as well. Applied voltage identifies large Cl-ion currents from the site of the loop passing through the pore. Rectification of the current of the Cl-ions is observed.

1. Introduction

Protein p7 from hepatitis C virus (HCV) belongs to the class of viral channel forming membrane proteins (VCPs) [1,2]. Together with other members of this class (e.g. reviewed in Ref. [3]), it shares the role of changing electrochemical and/or substrate gradients across the lipid membrane by forming an oligomeric assembly. The precise role within

* Corresponding author at: Institute of Biophotonics, School of Biomedical Science and Engineering, National Yang-Ming University, 155, Li-Non St., Sec. 2, Taipei, 112, Taiwan. Tel.: +886 2 2826 7394; fax: +886 2 28235460.
E-mail address: wfischer@ym.edu.tw (W.B. Fischer).

http://dx.doi.org/10.1016/j.bpc.2014.06.001
0301-4622/

the life cycle of the virus is still to debate, which is also a fact it has in common with most of the today's known viral channel proteins.

The protein is expressed within a polyprotein precursor from which it is cleaved, together with the other proteins of HCV genome, *via* cellular and viral proteases [4–6]. As a polytopic membrane protein of 63 amino acids with two transmembrane domains (TMDs), its termini are located towards the lumen of the endoplasmic reticulum [7]. Its role within the life cycle of HCV is envisaged to be similar to that of M2 of influenza A, supporting the release of the virion when trapped within the endosome during viral entry process [8,9]. It is proposed that p7 is present in the membrane of the virion [10,11].

It has been shown that p7 conducts ions [12–14] as well as protons [15]. Experiments have mostly been done with full length peptides expressed and purified from *Escherichia coli* [13] or produced from solid phase peptide synthesis [12,14] and reconstituted into artificial lipid bilayers. Proton conductance experiments have been done with vesicles extracted from cells measuring proton permeability as well as cell based imaging of vesicular pH [15].

Structural information has emerged from solid state [10,16] and solution NMR spectroscopy [17–19]. On the monomeric level, the structures either propose two anti-parallel aligned TMDs or a clamp-like overall structure. The fact that parallel aligned models are obtained for proteins with the amino acid sequence according to genotypes, 1a and 1b, and the clamp-like structure from proteins according to genotype 5a [18], drives a debate of structural differences albeit high sequence homology. Genotype dependent results have been derived when generating samples to be used for cryo-electron microscopy (EM) experiments [13,20,21]. Hexameric bundles are found for JFH-1 2a strains [21], while p7 of J4 1b strain is found in both, a hexameric [13] and heptameric formation [20].

Having a highly vital role within the life-cycle of HCV in chimpanzees [22] and in cell cultures [23,24], the protein emerges as a potential drug target. Most recent investigations have identified small molecule drugs to be able to block channel activity of p7 [10,12–14,25], with one used in clinical trials [25]. Poses of the drugs on the monomeric p7 protein are proposed to be within bundle models [10] or at either side when dealing with monomers [19,26].

In a combined bioinformatics and computational modeling approach, an antiparallel aligned model of full length p7 has been proposed ahead of available experimental data as mentioned above and modeled into a hexamer [27]. In the bundle model a histidine at position 17 is suggested to face the lumen of the pore, which is in agreement with the aforementioned NMR data. Extensive molecular dynamics simulations have been performed on both, hexameric and heptameric bundles, suggesting structural plasticity for the mechanism of function of p7 [28]. The model for the bundles based on p7 of genotype 1b has been derived from a monomeric p7 model obtained from NMR spectroscopy [17], copied and centered around a central axis either strictly according to the NMR coordinates or with optimized inter-subunit contacts.

At this stage, the mechanism of ion and/or proton conductance of the p7 bundle is still to be elucidated. With the structural information at hand, the mechanism of function in respect to ions is ready to be investigated computationally.

In this study, a structure based model of p7 monomer is taken [26], copied and assembled into a hexamer using established protocols [29,30]. The protein is embedded into a lipid bilayer. The protein/lipid system is hydrated also in such a way that it is embedded in electrolytes at a concentration of 1 M. The location of ions within the bundle is monitored in dependence of the number of protonated histidines and under applied physiological relevant voltages.

2. Materials and methods

The p7 protein sequence was taken from the HCV genotype 1a, H77 strain [12]: ALENLVILNA^{10} ASLAGTHGLV^{20} SFLVFFCFAW^{30} YLKGRWVPGA^{40} VYAFYGMWPL^{50} LLLLLALPQR^{60} AYA.

2.1. Assembly of the bundles

The monomeric structure of p7 was assembled from the individual TMDs as reported in detail earlier [26]. In brief, each of the TMDs (TMD1: 1–32, TMD2: 36–63) was individually simulated in a fully hydrated lipid bilayer (POPC) for 50 ns. Averaged structures over the backbone atoms of the 50 ns MD simulations of each of the TMDs were derived by fitting the peptide structure of each time frame to the starting structure thereby removing rotational and translational motions. The program g_covar from the GROMACS-4.0.5 packages was used for the calculations. Applying the same assembly protocol as mentioned below, the lowest energy structure of the assembled TMDs was generated. Finally, the monomer is formed by linking the assembled TMDs with a short loop (Lys-33, Gly-34, Arg-35) using the program Loopy [31,32]. The derived monomeric structure was embedded in a fully hydrated lipid bilayer and equilibrated in a 150 ns MD simulation.

Hexameric bundles were generated with the monomer by creating symmetric copies of the monomeric subunit around a central pore axis [29,30]. To sample the whole conformational space of the bundles each of the degrees of freedom was varied stepwise: (i) distance of the monomer to the central axis in steps of 0.25 Å covering 9 to 15 Å; (ii) rotational angle in steps of 5° covering 360°; (iii) tilt in steps of 2° covering −36° to +36°. For each position, the side chains were linked to the backbone. The side chain conformation was chosen to be the most likely one for a given backbone conformation according to the MOE library. A short minimization (15 steps of steepest decent) followed the generation of the side chains. For each conformation the potential energy was evaluated according to the all-atom AMBER94 force field mimicking a bilayer environment ($\varepsilon = 2$). The lowest energy conformer was embedded into fully hydrated POPC lipid bilayer.

2.2. MD simulations of the bundles

Lipid bilayer patches were generated from 16:1 to 18:1 Diester PC, 1-Palmitoyl-2-Oleoyl-sn-Glycero-3-Phosphocholine (POPC) molecules on the basis of the parameters of Chandrasekhar et al. [33]. The lipid patches were equilibrated for 50 ns. The hexameric bundles system has 512 lipid and 28215 water molecules. The lipid patches were equilibrated for 50 ns.

MD simulations of the bundles/lipid/water system were carried out with GROMACS-4.5.4 using Gromos96 ffG45a3 force field (geometric combination rule). The temperature of the peptide, lipid and the water molecules was separately coupled to a Berendsen thermostat at 310 K with a coupling time of 0.1 ps. Semi-isotropic pressure coupling was applied with a coupling time of 1.0 ps and a compressibility $4.5 \cdot 10^{-5}$ bar^{-1}. Long range electrostatics have been calculated using particle-mesh Ewald (PME) algorithm with grid dimensions of 0.12 nm. Lennard–Jones and short-range Coulomb interactions were cut off at 1.4 and 1 nm, respectively.

The p7 models were embedded into the POPC bilayer system and the overlapping lipid molecules were removed using the g_membed program from GROMACS-4.5.4. The hydrated system underwent 5000 steps of steepest decent and 5000 steps of conjugated gradient minimization to remove unfavorable interactions and equilibration for a total of 7.9 ns. Equilibration was achieved by gradually increasing the temperature from 100 K to 200 K and then to 310 K, while keeping the protein fully restraint applying position restraints with $k =$ 1000 KJ mol^{-1} nm^{-2}. The first two simulations (100 K and 200 K) were run for 200 ps, and the last simulation (310 K) was run for 1.5 ns. Holding the system at 310 K, the restrained protein was released in 4 consecutive 1.5 ns MD simulations reducing the force constant k ($k =$ 500 KJ mol^{-1} nm^{-2}, $k = 250$ KJ mol^{-1} nm^{-2}, $k = 100$ KJ mol^{-1} nm^{-2}, $k = 25$ KJ mol^{-1} nm^{-2}).

2.3. Histidine protonation

The program "protonate 3D" of the MOE suite was used to assign protonation states to the p7 bundle in dependence of various pH values. The pdb2gmx program from GROMACS was used to protonate the histidines of the unprotonated p7 bundle (H0). Protonated p7 structures were created with either three histidines alternately protonated (H3+) or all histidines protonated (H6+).

2.4. Adding ions

The protein–lipid systems H0 and H6+ were taken from the last frame of a 7.9 ns equilibration simulation. The genion program from GROMACS was used to replace water molecules with K-ions (OPLS-AA/L 2001), Na-, Ca- and Cl-ions. The aqueous compartments in these two models contained ~26,000 water molecules. The electrolyte concentration of the p7 hexamer system was set to 1.0 mol/L, corresponding to 491 K- or Na-ions and 503 Cl-ions (491 Ca-ions, 994 Cl-ions) in each of the neutralized compartments. After adding ions to the system, each simulation system was equilibrated another 1.5 ns and submitted to the production run for 200 ns.

2.5. Application of electric fields

In the p7 hexamer protein–lipid–1 M ion system, an external electric field was applied perpendicular to the membrane plane to maintain a fixed potential difference across the bilayer [34]. The p7 hexamer models were taken after equilibration. Electric fields (E) were applied as −/+0.0033 V/nm, −/+0.066 V/nm, −/+0.033 V/nm, −/+0,133 V/nm, −/+0.2 V/nm, −/+0.266 V/nm and −/+0.33 V/nm in the z-direction of the simulation box. Voltages (V) across the lipid membrane were calculated taking the membrane thickness ($d = 3$ nm) into account: $V = d \cdot E$.

2.6. Hardware equipment and analysis software

The simulations were run on a DELL i7-930 workstation, 28 core Opteron based computer cluster with Infiniband interconnects and the ALPS-Acer AR585 F1 Cluster in National Center for High-Performance Computing (NCHC). Plot and pictures were made with VMD 1.9 and MOE suit (www.chemcomp.com).

3. Results

A monomeric p7 protein is generated in a four step procedure, (i) generation of two ideal helices, (ii) equilibrating the helices *via* MD simulations, (iii) connecting the two helices *via* the linker sequence of the protein, generating the monomer (Supplemental Fig. 1) [26], and (iv) assembling the monomer into hexameric bundles (Fig. 1). MD simulations of the monomer (150 ns) and the bundles (200 ns each) generate stable structures since the RMSD values of all simulations are leveling off after a short initial rise (Supplemental Fig. 2A). The RMSF values of the monomer indicate fluctuating residues within the core region of TMD1 (His-17, Gly-18, Leu-19, Val-20, Ser-21) as well as for the first 8 amino acids and the loop region (Supplemental Fig. 2B).

Three types of bundles are simulated: without any of the histidines being protonated (H0) (Fig. 1, I), with histidines being alternately protonated and unprotonated (H3+) (Fig. 1, II) and with all of the histidines protonated (H6+) (Fig. 1, III). The protonation states of H0 and H6+ correspond to an estimated pH of more than ~6.5 and less than ~6.0, respectively (Supplemental Fig. 3). The most important intermediate protonation state is found to be H3+. The RMSD values of the bundles level off after the first 10 ns (Supplemental Fig. 2C). While for the unprotonated bundle the lumen of the pore collapses, the protonated bundles remain "open" on the level of the histidines (Fig. 1B). The phenylalanine residues of TMD1 (especially Phe-25 and -28) amass in the lumen towards the side of the loops (Fig. 1B). No continuous water column is observed after the collapse of the bundle.

The tilt and kink are calculated for the individual TMDs of each of the bundles H0, H3+ and H6+ from the 200 ns MD simulations (Supplemental Table 1). Averaged tilts of these TMDs, inner (TMD1s) and outer (TMD2s) helices, are within a range of 15.8° to 20.1° for all the bundles, H0, H3+ and H6+. The kink angles of the inner helices are larger (26.1° to 34.5°) than the kink angles of the outer helices (13.3° to 19.2°) independent of the protonation state of the histidine residues.

Comparing among the bundles, the tilt angles of the TMD1s are slightly larger in H6+ than in H0 (19.8 (H6+) compared to 18.3° (H0), t-test: 1.7). The kink of the TMD1s is more straight in H6+ than in H0 (26.1° (H6+) compared to 34.1° (H0), t-test: 4.2). Structurally distinct features are compensated by the inner ring of TMDs (TMD1).

The Cl-ions, which have to be added to neutralize the box, accumulate in H3+ and H6+ at the site of the protonated histidine residues (Fig. 2A). Counting the positions along the z-coordinate of the Cl-ions reveals that many of them are found in close proximity of the loops independent of the protonation state of His-17 (Fig. 2B). Upon protonation, the dwell time of the Cl-ions within the lumen of the pore increases with the number of histidines protonated. The Cl-ions gain access to the histidines *via* the site of the termini. In H3+, Cl-ions accumulate around the unprotonated histidine residues to a lesser extent than around the protonated residues (Fig. 2C, left). The number of Cl-ions within the lumen of the pore can be higher than 6 nm^{-2}, positioning themselves at the charged histidines (Fig. 2C). The histidines are not in a planar architecture for H3+. The dwell time at the three charged histidines (red spot in Fig. 2C, left) is larger in comparison to the dwell time around the uncharged histidines (light spot in Fig. 2C, left). In the case of H6+, the non-planar architecture is seen by the spread of the density in the z-direction (Fig. 2C, right).

Embedding the lipid/H0 system into a '1 molar aqueous solution' of either KCl, NaCl or $CaCl_2$ shows stable RMSD curves after about 10 ns (Supplemental Fig. 2D). There are no signs of the cations to enter the H0-bundle when embedded in NaCl or KCl solution (Supplemental Fig. 4A/B). In the case of a $CaCl_2$ solution both, a Ca-ion and a Cl-ion are trapped in the pore (Supplemental Fig. 4C) so that they are placed in the order histidines – Ca-ion – Cl-ion (Fig. 3A), with the Cl-ion facing the loop region. Simulations in the presence of H6+ reveal (for RMSD curves see Supplemental Fig. 2E) that cations are not present in the bundle but Cl-ions, which enter and exit the pore at the side of the termini, and are predominantly located around the histidine residues (Supplemental Fig. 4D–F).

Calculation of the mean life time of the overall shape from the radius of gyration reveals that H0 collapses much faster ((1.7 ± 01) ns) than H3+ ((7.2 ± 0.3) ns) and H6+ ((7.1 ± 0.2) ns) (Fig. 3B and Supplemental Table 2). The latter two adopt an almost similar mean life time. Comparative calculations for the other H0 bundles in the presence of 1 molar salt solution as discussed above reveal that in the presence of Ca- and Cl-ions, as in the H0 simulation in 1 M $CaCl_2$ solution, the bundle collapses slightly faster with life time of (1.1 ± 0.1) ns (Supplemental Fig. 5A and Table 2). A similar trend is found for simulations of H6+ in the same 1 M solutions (Supplemental Fig. 5B and Table 2). The diffuse presence of Cl-ions leads to a prolonged maintenance of the shape compared to H0 (1 M NaCl (3.2 ± 0.1) ns, 1 M KCl (3.3 ± 0.1) ns). In comparison with H6+ simulations, the shape collapses slightly faster except for H6+in 1 M $CaCl_2$ solution ((9.4 ± 0.5) ns). Thus, the presence of ions within the pore affects the shape and the dynamics of protein motion within the bundle.

Application of various voltages to the lipid/H0 system embedded in 1 molar solutions of either KCl or $CaCl_2$ reveals a slightly rectifying behavior of the bundle (Fig. 4). In a range from −200 mV to +200 mV no ions are crossing the bundles in the KCl solution. Conductance of Ca-ions is found also at low voltages. There is a tendency of higher $CaCl_2$ conductance over KCl. Negative voltage, which corresponds to the movement of Cl-ions from the occupied loop regions (see Fig. 2B)

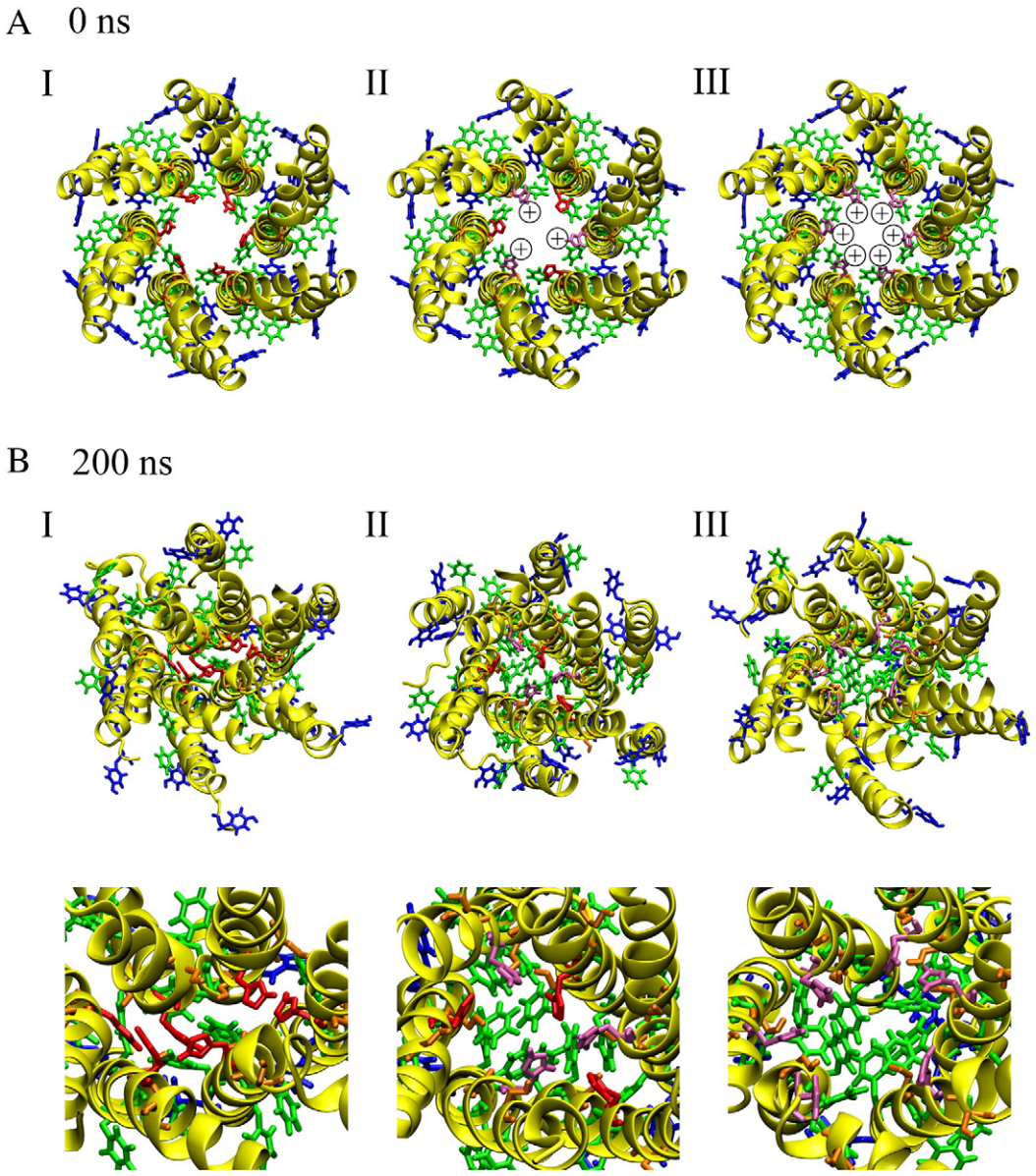

Fig. 1. (A) The hexameric bundle generated from the monomer is shown with histidine residues unprotonated (I, H0), alternately protonated (II, H3+) and fully protonated (III, H6+) at 0 ns and 200 ns (B). The backbone is shown as yellow cartoon, with the side chains shown in stick mode and color coded as the following: Ser-12 (orange), His-17 (red), protonated His-17 (pink), Tyr-31, -42, -45, and -62 (dark blue), Phe-22, -25, -26, -28, and -44 (green).

into the bundle, leads to a larger number of ions crossing in the respective directions as from the termini side, suggesting rectification. A similar tendency is not observed for the cations. It is observed that cations and anions cross the bundle simultaneously. At higher voltage (±1000 mV) the bundles collapse resulting in increasing RMSD values (Supplemental Fig. 2F and G).

4. Discussion

4.1. Protein and ion dynamics

The concept of two almost parallel aligned TMDs of p7 is experimentally supported [16–19,35]. Different architectures of the TMDs allow for different dynamics and protein mechanics. The crowding of the aromatic residues towards the loop region [17,19] is responsible for the large kink in TMD1. The calculated tilt and kink data suggest a straight ring of outer helices compared to a more kinked inner ring. The inner ring readily adapts to the electrostatic conditions within the lumen of the pore. The geometries obtained in this study match structure proposals from solid state NMR spectroscopy [16,35]: two large TMDs are found each consisting of two helical sub-domains. The tilt of the large TMDs is measured to be 25° and 10°, corresponding to TMD1 and TMD2, respectively. The latter tilt is attributed to one of the helical sub-domains which consist of residues Leu-50 to Leu-57. Since the first large TMD is longer than the second, the larger tilt of 25° is also correlated with a kinked TMD. Thus, TMD1 should have a larger kink than TMD2, which is consistent with the data presented in this study. Also, in a recently reported hexameric p7 bundle (5a strain), suggesting a 'clamp-like' monomeric architecture for the monomer, TMD1 is highly kinked [18]. Simulations in this study with decreasing pH simulated by fixed charges on His-17 reveal that the kink could act as a gate by stretching out upon protonation.

Models proposed from a combination of NMR spectroscopic data and MD simulations reveal upright helices in POPC bilayers which also optimizes packing during the MD simulations [28]. A hexameric model, constructed by copying the NMR-based monomer into a cyclic

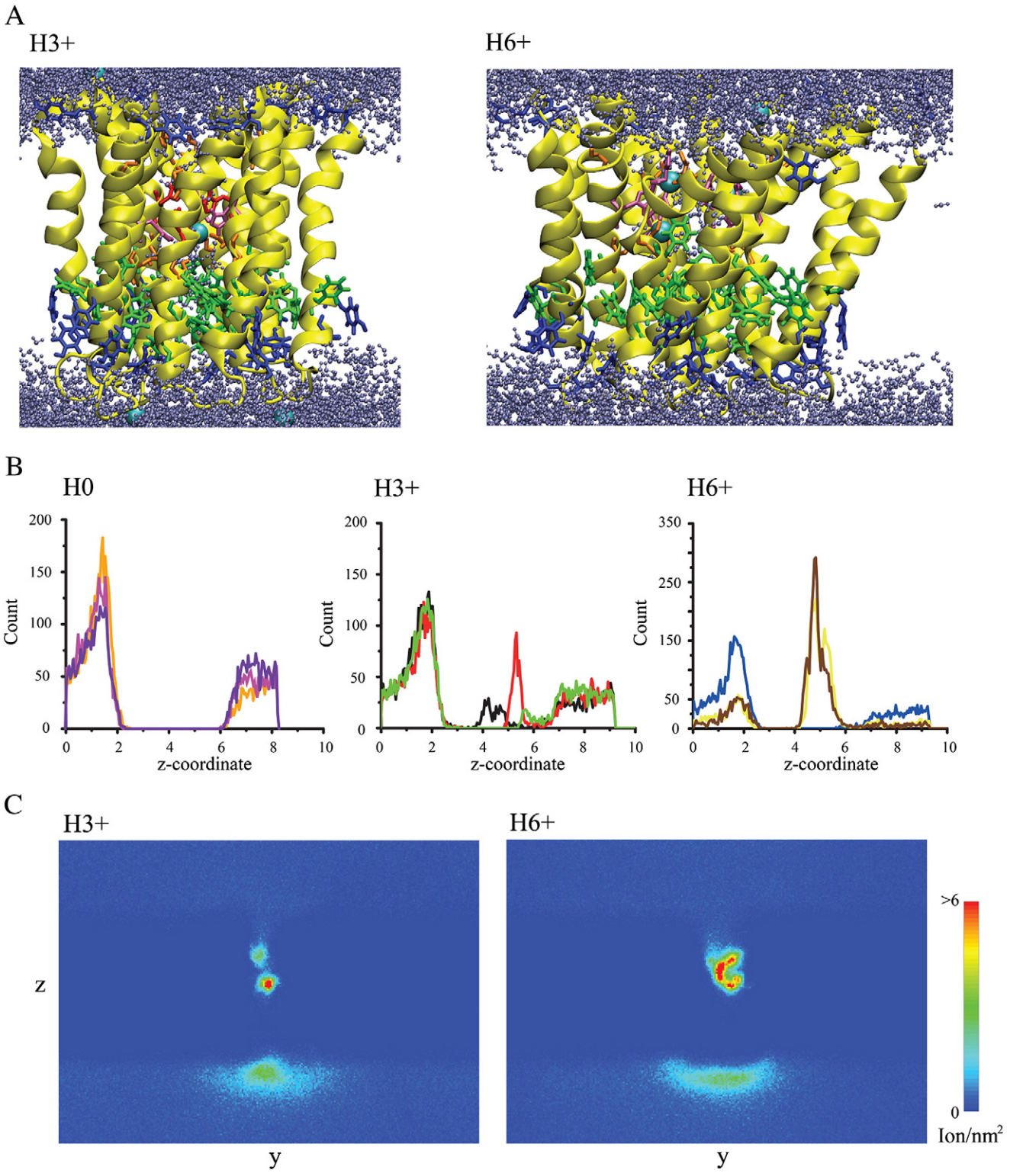

Fig. 2. (A) Models of 3× protonated (H3+, left) and fully protonated p7 bundle (H6+, right). Lipid molecules are omitted for clarity; water molecules are shown in blue. Backbones are shown in yellow; amino acids are shown in stick mode as the following: Ser-12 (orange), His-17 (red), protonated His-17 (pink), Tyr-31, -42, -45, and -62 (dark blue), Phe-22, -25, -26, -28, and -44 (green). (B) Histogram analysis of the position of three representative Cl-ions from each of the simulations with unprotonated p7 bundle (H0, left), H3+(middle) and H6+ (right). (C) Cl-ion density map from the simulations with H3+ (left) and H6+ (right) in a side view representation (view from inside the membrane). The density is shown as ion per nm^2, with blue indicative for 0 ions per nm^2 and red indicative for 6 or more ions per nm^2.

way, also tends to collapse during equilibration but not when a heptameric arrangement used. Packing optimized heptameric and hexameric models are reported to be stable. Overall, all stable models allow ions to flow across the protein under applied voltage.

4.2. Modeling ion current

A series of structure based computational methods is available to assess ion flux through channels and pores. Simulations undertaken in the

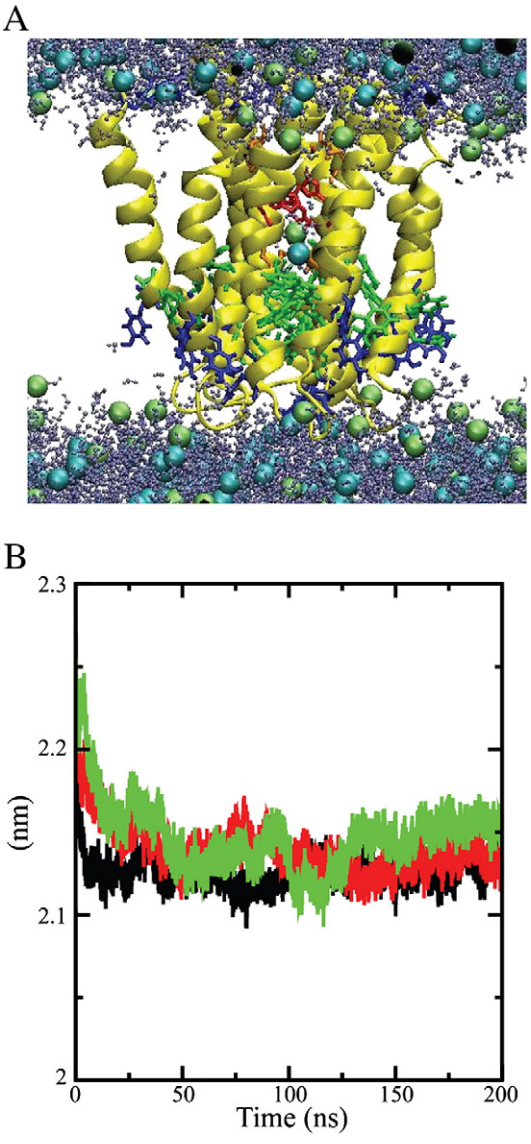

Fig. 3. (A) Bundle of unprotonated p7 (H0) in the presence of a 1 M solution of $CaCl_2$. The Ca-ions (green) and the Cl-ions (blue) are shown as spheres. Lipid molecules are omitted for clarity; water molecules are shown in blue. Backbones are shown in yellow; amino acids are shown in stick mode as the following: Ser-12 (orange), His-17 (red), Tyr-31, -42, -45, and -62 (dark blue), Phe-22, -25, -26, -28, and -44 (green). (B) Radius of gyration of the three bundles H0 (black line), H3+(red line) and H6+(green line) during the 200 ns MD simulation.

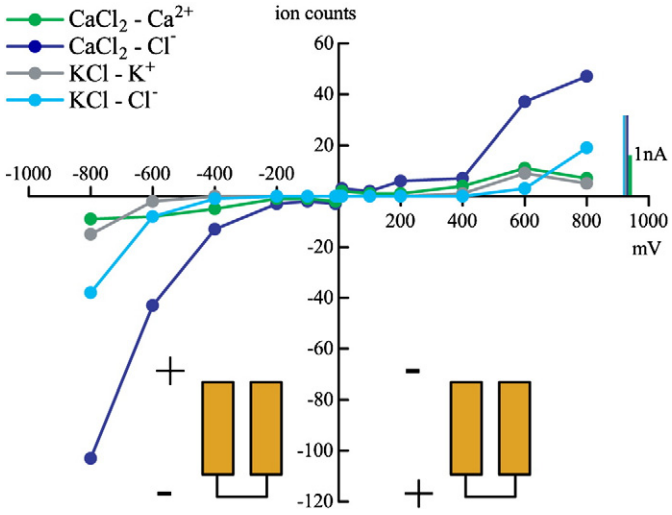

Fig. 4. Transitions of mono and divalent ions through the p7 bundle H0 as a function of various voltages applied. Solutions have been either 1 M KCl or $CaCl_2$. Gray and blue lines represent K-ion and Cl-ion, respectively; green and dark blue lines represent Ca-ion and the respective Cl-ion. The indicated current is estimated according to $I = \Delta Q/\Delta t = z \cdot e \cdot (\text{ion counts})/\Delta t$ with $\Delta t = 5$ ns, $|z_{Na+/K+/Cl-}| = 1$ and $z_{Ca2+} = 2$.

presence of an applied voltage have led to a conductance pattern of the viral channel p7 of HCV [28], bacterial voltage-gated sodium channel [36], an acid inducible channel [37] and other channels [38], to mention only some of the work. Other methods supplement the endeavor, using e.g. a double membrane system [39] or calculate the potential of mean force (PMF) of ions along the lumen of ion channels [40,41]. In recent studies, a direct comparison of the two attempts is reported (see Ref. [38], for another viral channel protein).

In the present study, a high concentration of salt is used. Previous studies have shown that certain force field parameters cause large aggregations of ions when simulating these high concentrations [42]. The formation of these aggregates is, however, not reported for the force field parameters used in this study applying the geometric combination rule [43]. Furthermore, the computed ion–ion radial distribution functions (data not shown) and visual inspection of the trajectories do not reveal any ion aggregation.

In the present study, no ions of the KCl solution and only very few ions of the $CaCl_2$ solution cross the pore under applied voltage comparable to experimental condition (~100 mV). Since the transition of 1 monovalent ion in 5 ns already leads to an estimated current of 32 pA corresponding to a conductance of 320 pS at 100 mV, the experimentally found conductance (e.g. 14 pS [14], >35 pS [17], and 86 pS [12], all in 0.5 M KCl buffer at various holding potentials) cannot be reproduced accurately. The observation of only very few ion transitions is in agreement with these experimental data. When applying a voltage of ±1000 mV, the pore of the hexameric bundle widens and the entire system destabilizes. In another simulation study, a conductance of 236 pS was calculated for a hexameric p7 model at 1500 mV [28] which might refer to a voltage over the entire simulation box. Since, in the present study, the potential difference is calculated over the lipid membrane, the different results might be in agreement using the same conventions.

Similar to the presented data, a low rectifying behavior of p7 has been shown also experimentally suggesting that p7 proteins insert in a preferred orientation in the membrane [17]. Combining those experimental data and the presented simulations, it can be concluded that p7 inserts first with the termini site into the membrane.

The present data suggest a larger anion than cation flux. This fact explains the low cation specificity suggesting a considerable anion flux *in vivo*. With a larger flux from the putative inside of a virion due to the slightly larger current going from the loop side into the pore, the protein as a pore could regulate the Cl-ion density within the virion.

4.3. Cl-ion (and cation) flux

The data from the voltage experiments catalyze the following thoughts. The movement is somewhat different as expected. With the existence of ions along the pore from the termini site (Fig. 2B), one could anticipate that it just needs voltage to pass further. Under applied voltage however, it is the Cl-ions at the site of the loop which seem to enter the pore more readily. It is therefore concluded that trapping the ions in the loop region by Lys-33 and Arg-35 is an important step to lead to an ion entry. In simulations of a model of the ryanodine receptor (RyR), it has been suggested that Ca-ions 'migrate' along the surface of the pore prior to pore entry [44]. One can speculate that with such a step the loss of entropy (ion mobility) is compensated by the gain of

binding enthalpy (eventually partial stripping-off of the hydration shell and replacing water-ion contacts by side-chain ion contacts) before the ion enters the pore. In case of the termini side, the dynamics of the helices may prevent an energetically favorable entry. Implementing experimental data on the dynamics of the individual helices of p7 from solid state NMR spectroscopy [16], TMD1 has a mobile helical segment at the immediate N terminal side and a more rigid helix towards the C terminal side. Another dynamic helical region is reported for the N terminal side of TMD2 with a more rigid helix towards the N terminal side. The dynamical part of TMD1 prevents the ion flux in as much as it would possibly need to become less dynamic during ion permeation. The dynamical part of TMD2 could be essential for gating, 'opening' the pore and enabling the accumulated ions to pass.

Cl-ion flux direction could help lowering any mobile negative charges which are crowding in during the formation of the virion.

In the simulations, it is found that cations and anions pass each other within the pore, a finding which has been suggested to explain experimentally derived conductance data for Vpu of HIV-1 when reconstituted into lipid bilayers [45].

4.4. Ca-ions within the pore

With Ca-ions found in the unprotonated bundle it is anticipated that Ca-ions serve as stabilizing factors within the bundle. Since Cl-ions are also present within the bundle, especially when protonated, the combination of the two would lead to a stabilization of the bundle within a certain pH range. Of course, if 'fully' protonated, the cation should leave the bundle.

It has been reported that the addition of Cu-ion (2+) blocks channel activity of p7 [46] and also M2 of influenza A [47]. In the light of the present study, the Cu-ions form much more stable complexes with the histidines [48,49] than e.g. Ca-ions [50] and by this induce conformational restraints due to the formation of stable square planar complexes, which are not only found with just histidines but also within proteins [48,51,52], preventing channel activity.

4.5. Histidines and phenylalanines

In most of the simulations the histidines do not maintain a 'planar' geometry; they rather adopt staggered conformations. In as much as the planar ring-like geometry of the histidine residues is the guarantor for p7 proton conductance [15], similar to the ring of histidines proposed for M2 of influenza A [53–56], this needs to be evaluated.

The clustering of Phe-25 and -28 could serve as a hydrophobic gate similar to those proposed for the nicotinic acetylcholine receptor [57]. At this stage it is still speculative whether the phenylalanines have structure stabilizing effects or even contribute to the selectivity of the channel [28].

Summarizing the presented data, in the presence of localized point charges within the bundle due to the ring of histidines-17 the bundle harbors divalent ions such as Ca-ions. Upon protonation of the histidines, the pore architecture is suggested to collapse *via* conformational changes of the inner helices, TMD1s, forming a staggered arrangement of the histidines. The stacked arrangement could be seen as part of a putative proton shuttling mechanism. At low pH the bundle is suggested to conduct Cl-ions and positive ions simultaneously through the pore. The architecture of an inner and outer ring of helices relates distinct mechanics in response to environmental conditions to each ring of helices. Anions enter the pore from the positively charged loop site, thus it seems as if they need to be immobilized prior to pore entry.

5. Conclusion

A monomeric model of p7 from HCV is constructed and assembled into a hexameric structure. The resulting pore model is found to be in agreement with experimental data with regard to the geometry of the TMDs and the plausible position of His-17. The presence of a Ca-ion in the pore with unprotonated histidines corresponding to neutral pH suggests a functional role, e.g. stabilizing effect. Large Cl-ion currents passing through the p7 model are observed in simulations with applied voltage.

Immobilization of ions at the protein is essential for pore entry and results in a low rectification of Cl-ion currents. Comparison with experimental conductance measurements allows the conclusion that p7 inserts preferably with the termini site into the membrane.

Acknowledgement

W.B.F. thanks the National Science Council (NSC-98-2112-M-010-002-MY3), Taiwan, for financial support. R.F. thanks the German Excellence Initiative II — Global Networks for financial support. R.S. thanks the Heidelberg Medical School and the Baden-Württemberg Stiftung for a Ph.D. scholarship. We thank H.-J. Hsu, M.-H. Lin, M.M. Kalita and R.D. Mahato (Taipei, TW) for helpful discussions.

Appendix A. Supplementary data

Supplementary data to this article can be found online at http://dx.doi.org/10.1016/j.bpc.2014.06.001.

References

[1] W.B. Fischer, Y.-T. Wang, C. Schindler, C.-P. Chen, Mechanism of function of viral channel proteins and implications for drug development, Int. Rev. Cell Mol. Biol. 294 (2012) 259–321.
[2] J.L. Nieva, V. Madan, L. Carrasco, Viroporins: structure and biological functions, Nat. Rev. Microbiol. 10 (2012) 563–574.
[3] K. Wang, S. Xie, B. Sun, Viral proteins function as ion channels, Biochim. Biophys. Acta 1808 (2010) 510–515.
[4] C. Lin, B.D. Lindenbach, B.M. Pragai, D.W. McCourt, C.M. Rice, Processing in the hepatitis C virus E2-NS2 region: identification of p7 and two distinct E2-specific products with different C termini, J. Virol. 68 (1994) 5063–5073.
[5] M.E. Major, S.M. Feinstone, The molecular virology of hepatitis C, Hepatology 25 (1997) 1527–1538.
[6] S. Khaliq, S. Jahan, S. Hassan, Hepatitis C virus p7: molecular function and importance in hepatitis C virus life cycle and potential antiviral target, Liver Int. 31 (2011) 606–617.
[7] S. Carrère-Kremer, C. Montpellier-Pala, L. Cocquerel, C. Wychowski, F. Penin, J. Dubuisson, Subcellular localization and topology of the p7 polypeptide of Hepatitis C virus, J. Virol. 76 (2002) 3720–3730.
[8] S. Griffin, C. StGelais, A.M. Owsianka, A.H. Patel, D. Rowlands, M. Harris, Genotype-dependent sensitivity of hepatitis C virus to inhibitors of the p7 ion channel, Hepatology 48 (2008) 1779–1790.
[9] S.D.C. Griffin, Plugging the holes in hepatitis C virus antiviral therapy, Proc. Natl. Acad. Sci. U. S. A. 106 (2009) 12567–12568.
[10] T.L. Foster, G.S. Thompson, A.P. Kalverda, J. Kankanala, M. Bentham, L.F. Wetherill, J. Thompson, A.M. Barker, D. Clarke, M. Noerenberg, A.R. Pearson, D.J. Rowlands, S.W. Homans, M. Harris, R. Foster, S. Griffin, Structure-guided design affirms inhibitors of hepatitis C virus p7 as a viable class of antivirals targeting virion release, Hepatology 59 (2014) 408–422.
[11] E. Atkins, R. Tatineni, H. Li, D. Gretch, M. Harris, S. Griffin, The stability of secreted, acid-labile H77/JFH-1 hepatitis C virus (HCV) particles is altered by patient isolate genotype 1a p7 sequences, Virology 448 (2014) 117–124.
[12] D. Pavlović, D.C.A. Neville, O. Argaud, B. Blumberg, R.A. Dwek, W.B. Fischer, N. Zitzmann, The hepatitis C virus p7 protein forms an ion channel that is inhibited by long-alkyl-chain iminosugar derivatives, Proc. Natl. Acad. Sci. U. S. A. 100 (2003) 6104–6108.
[13] S.D.C. Griffin, L.P. Beales, D.S. Clarke, O. Worsfold, S.D. Evans, J. Jäger, M.P.G. Harris, D.J. Rowlands, The p7 protein of hepatitis C virus forms an ion channel that is blocked by the antiviral drug, amantadine, FEBS Lett. 535 (2003) 34–38.
[14] A. Premkumar, L. Wilson, G.D. Ewart, P.W. Gage, Cation-selective ion channels formed by p7 of hepatitis C virus are blocked by hexamethylene amiloride, FEBS Lett. 557 (2004) 99–103.
[15] A.L. Wozniak, S. Griffin, D. Rowlands, M. Harris, M.-K. Yi, S.M. Lemon, S.A. Weinman, Intracellular proton conductance of the hepatitis C virus p7 protein and its contribution to infectious virus production, PLoS Pathog. 6 (2010) e1001087.
[16] G.A. Cook, S.J. Opella, Secondary structure, dynamics, and architecture of the p7 membrane protein from hepatitis C virus by NMR spectroscopy, Biochim. Biophys. Acta 1808 (2011) 1448–1453.
[17] R. Montserret, N. Saint, C. Vanbelle, A.G. Salvay, J.P. Simorre, C. Ebel, N. Sapay, J.-G. Renisio, A. Böckmann, E. Steinmann, T. Pietschmann, J. Dubuisson, C. Chipot, F. Penin, NMR structure and ion channel activity of the p7 protein from hepatitis C virus, J. Biol. Chem. 285 (2010) 31446–31461.

[18] B. OuYang, S. Xie, M.J. Berardi, X. Zhao, J. Dev, W. Yu, B. Sun, J.J. Chou, Unusual architecture of the p7 channel from hepatitis C virus, Nature 498 (2013) 521–525.
[19] G.A. Cook, L.A. Dawson, Y. Tian, S.J. Opella, Three-dimensional structure and interaction sudies of hepatitis C virus p7 in 1,2-dihexanoyl-sn-glycero-3-phosphatidylcholine by solution nuclear magnetic resonance, Biochemistry 52 (2013) 5295–5303.
[20] D. Clarke, S. Griffin, L. Beales, C.S. Gelais, S. Burgess, M. Harris, D. Rowlands, Evidence for the formation of a heptameric ion channel complex by the hepatitis C virus p7 protein in vitro, J. Biol. Chem. 281 (2006) 37057–37068.
[21] P. Luik, C. Chew, J. Aittoniemi, J. Chang, P. Wentworth Jr., R. Dwek, P.C. Biggin, C. Vénien-Bryan, N. Zitzmann, The 3-dimensional structure of the hepatitis C virus p7 ion channel by electron microscopy, Proc. Natl. Acad. Sci. U. S. A. 106 (2009) 12712–12716.
[22] A. Sakai, M. St. Claire, K. Faulk, S. Govindarajan, S.U. Emerson, R.H. Purcell, J. Bukh, The p7 polypeptide of hepatitis C virus is critical for infectivity and contains functionally important genotype-specific sequences, Proc. Natl. Acad. Sci. U. S. A. 100 (2003) 11646–11651.
[23] C.T. Jones, C.L. Murray, D.K. Eastman, J. Tassello, C.M. Rice, Hepatitis C virus p7 and NS2 proteins are essential for production of infectious virus, J. Virol. 81 (2007) 8374–8383.
[24] E. Steinmann, F. Penin, S. Kallis, A.H. Patel, R. Bartenschlager, T. Pietschmann, Hepatitis C virus p7 protein is crucial for assembly and release of infectious virions, PLoS Pathog. 3 (2007) 962–971.
[25] C.A. Luscombe, Z. Huang, M.G. Murray, M. Miller, J. Wilkinson, G.D. Ewart, A novel hepatitis C virus p7 ion channel inhibitor, BIT225, inhibits bovine viral diarrhea virus *in vitro* and shows synergism with recombinant interferon-a-2b and nucleaoside analogues, Antiviral Res. 86 (2010) 144–153.
[26] Y.-T. Wang, H.-J. Hsu, W.B. Fischer, Computational modeling of the p7 monomer from HCV and its interaction with small molecule drugs, Springer Plus 2 (2013) 324.
[27] G. Patargias, N. Zitzmann, R. Dwek, W.B. Fischer, Protein–protein interactions: modeling the hepatitis C virus ion channel p7, J. Med. Chem. 49 (2006) 648–655.
[28] D.E. Chandler, F. Penin, K. Schulten, C. Chipot, The p7 protein of hepatitis C virus forms structurally plastic, minimalist ion channels, PLoS Comput. Biol. 8 (2012) e1002702.
[29] J. Krüger, W.B. Fischer, Assembly of viral membrane proteins, J. Chem. Theory Comput. 5 (2009) 2503–2513.
[30] H.-J. Hsu, W.B. Fischer, In silico investigations of possible routes of assembly of ORF 3a from SARS-CoV, J. Mol. Model. 18 (2011) 501–514.
[31] Z. Xiang, C.S. Soto, B. Honig, Evaluating conformational free energies: the colony energy and its application to the problem of loop prediction, Proc. Natl. Acad. Sci. U. S. A. 99 (2002) 7432–7437.
[32] C.S. Soto, M. Fasnacht, J. Zhu, L. Forrest, B. Honig, Loop modeling: sampling, filtering, and scoring, Proteins 70 (2008) 834–843.
[33] I. Chandrasekhar, M. Kastenholz, R.D. Lins, C. Oostenbrink, L.D. Schuler, W.F. van Gunsteren, A consistent potential energy parameter set for lipids: dipalmitoylphosphatidylcholine as a benchmark of the GROMOS96 45A3 force field, Eur. Biophys. J. 32 (2003) 67–77.
[34] D.P. Tieleman, H. Leontiadou, A.E. Mark, S.J. Marrink, Simulation of pore formation in lipid bilayers by mechanical stress and electric fields, J. Am. Chem. Soc. 125 (2003) 6382–6383.
[35] G.A. Cook, S.J. Opella, NMR studies of the p7 protein from hepatitis C virus, Eur. Biophys. J. 39 (2010) 1097–1104.
[36] M.B. Ulmschneider, C. Bagnéris, E.C. McCusker, P.G. DeCaen, M. Delling, D.E. Clapham, J.P. Ulmschneider, B.A. Wallace, Molecular dynamics of ion transport through the open conformation of a bacterial voltage-gated sodium channel, Proc. Natl. Acad. Sci. U. S. A. 110 (2013) 6364–6369.
[37] J. Lu, N. Modi, U. Kleinekathöfer, Simulation of ion transport through an N-acetylneuraminic acid-inducible membrane channel: from understanding to engineering, J. Phys. Chem. B 117 (2013) 15966–15975.
[38] M.A. Wilson, C. Wei, P. Bjelkmar, B.A. Wallace, A. Pohorille, Molecular dynamics simulation of the antiamoebin ion channel: linking structure and conductance, Biophys. J. 100 (2011) 2394–2402.
[39] C. Kutzner, H. Grubmüller, B.L. de Groot, U. Zachariae, Computational electrophysiology: the molecular dynamics of ion channel permeation and selectivity in atomistic detail, Biophys. J. 101 (2011) 809–817.
[40] T.W. Allen, O.S. Andersen, B. Roux, Molecular dynamics — potential of mean force calculations as a tool for understanding ion permeation and selectivity in narrow channels, Biophys. Chem. 124 (2006) 251–267.
[41] J.S. Hub, B.L. de Groot, Mechanism of selectivity in aquaporins and aquaglycoporins, Proc. Natl. Acad. Sci. U. S. A. 105 (2008) 1198–1203.
[42] P. Auffinger, T.E. Cheatham III, A.C. Vaiana, Spontaneous formation of KCl aggregates in biomolecular simulations: a force field issue? J. Chem. Theory Comput. 3 (2007) 1851–1859.
[43] A. Cordomi, O. Edholm, J.J. Perez, Effect of force field parameters on sodium and potassium ion binding to dipalmitoyl phosphatidylcholine bilayers, J. Chem. Theory Comput. 5 (2009) 2125–2134.
[44] R. Schilling, R.H.A. Fink, W.B. Fischer, MD simulation of the central pore of ryanodine receptors and sequence comparison with 2B protein from coxsackie virus, Biochim. Biophys. Acta 1838 (2014) 1122–1131.
[45] T. Mehnert, A. Routh, P.J. Judge, Y.H. Lam, D. Fischer, A. Watts, W.B. Fischer, Biophysical characterisation of Vpu from HIV-1 suggests a channel-pore dualism, Proteins 70 (2008) 1488–1497.
[46] C.F. Chew, R. Vijayan, J. Chang, N. Zitzmann, P.C. Biggin, Determination of pore-lining residues in the hepatitis C virus p7 protein, Biophys. J. 96 (2009) L10–L12.
[47] C.S. Gandhi, K. Shuck, J.D. Lear, G.R. Dieckmann, W.F. DeGrado, R.A. Lamb, L.H. Pinto, Cu(II) inhibition of the proton translocation machinery of the influenza A virus M2 protein, J. Biol. Chem. 274 (1999) 5474–5482.
[48] J.H. Viles, F.E. Cohen, S.B. Prusiner, D.B. Goodin, P.E. Wright, H.J. Dyson, Copper binding to the prion protein: structural implications of four identical cooperative binding sites, Proc. Natl. Acad. Sci. U. S. A. 96 (1999) 2042–2047.
[49] J.T. Rubino, K.J. Franz, Coordination chemistry of copper proteins: how nature handles a toxic cargo for essential function, J. Inorg. Biochem. 107 (2012) 129–143.
[50] S.-M. Liao, Q.-S. Du, J.-Z. Meng, Z.-W. Pang, R.-B. Huang, The multiple roles of histidine in protein interactions, Chem. Cent. J. 7 (2013) 44.
[51] W.R. Walker, Y.-H. Shaw, N.C. Li, Histidine and histamine complexes of copper and zinc, J. Coord. Chem. 3 (1973) 77–84.
[52] H. Kozlowski, M. Łuczkowski, M. Remelli, Prion proteins and copper ions. Biological and chemical controversies. Dalton Trans. 39 (2010) 6371–6385.
[53] L.H. Pinto, G.R. Dieckmann, C.S. Gandhi, C.G. Papworth, J. Braman, M.A. Shaughnessy, J.D. Lear, R.A. Lamb, W.F. DeGrado, A functionally defined model for the M2 proton channel of influenza A virus suggests a mechanism for its ion selectivity, Proc. Natl. Acad. Sci. U. S. A. 94 (1997) 11301–11306.
[54] J. Wang, S. Kim, F. Kovacs, T.A. Cross, Structure of the transmembrane region of the M2 protein H^+ channel, Protein Sci. 10 (2001) 2241–2250.
[55] J. Hu, R. Fu, K. Nishimura, L. Zhang, H.-X. Zhou, D.D. Busath, V. Vijayvergiya, T.A. Cross, Histidines, heart of the hydrogen ion channel from influenza A virus: towards an understanding of conductance and proton selectivity, Proc. Natl. Acad. Sci. U. S. A. 103 (2006) 6865–6870.
[56] J.R. Schnell, J.J. Chou, Structure and mechanism of the M2 proton channel of influenza A virus, Nature 451 (2008) 591–595.
[57] A. Miyazawa, Y. Fujiyoshi, N. Unwin, Structure and gating mechanism of the acetylcholine receptor pore, Nature 423 (2003) 949–955.